ACS APPLIED MATERIALS & INTERFACES

Subscriber access provided by SYNCHROTRON RADIATION RES CTR

Article

Live Templates of a Supramolecular Block Copolymer for the Synthesis of Ordered Nanostructured TiO Films via Guest Exchange

Wei-Tsung Chuang, Yan-Ming Hsu, En-Li Lin, I-Ming Lin, Ya-Sen Sun, Yeo-Wan Chiang, Chun-Jen Su, Yao-Chang Lee, and U-Ser Jeng

ACS Appl. Mater. Interfaces, **Just Accepted Manuscript** • DOI: 10.1021/acsami.6b12216 • Publication Date (Web): 16 Nov 2016

Downloaded from http://pubs.acs.org on November 22, 2016

Just Accepted

"Just Accepted" manuscripts have been peer-reviewed and accepted for publication. They are posted online prior to technical editing, formatting for publication and author proofing. The American Chemical Society provides "Just Accepted" as a free service to the research community to expedite the dissemination of scientific material as soon as possible after acceptance. "Just Accepted" manuscripts appear in full in PDF format accompanied by an HTML abstract. "Just Accepted" manuscripts have been fully peer reviewed, but should not be considered the official version of record. They are accessible to all readers and citable by the Digital Object Identifier (DOI®). "Just Accepted" is an optional service offered to authors. Therefore, the "Just Accepted" Web site may not include all articles that will be published in the journal. After a manuscript is technically edited and formatted, it will be removed from the "Just Accepted" Web site and published as an ASAP article. Note that technical editing may introduce minor changes to the manuscript text and/or graphics which could affect content, and all legal disclaimers and ethical guidelines that apply to the journal pertain. ACS cannot be held responsible for errors or consequences arising from the use of information contained in these "Just Accepted" manuscripts.

ACS Publications

ACS Applied Materials & Interfaces is published by the American Chemical Society.
1155 Sixteenth Street N.W., Washington, DC 20036

Published by American Chemical Society. Copyright © American Chemical Society. However, no copyright claim is made to original U.S. Government works, or works produced by employees of any Commonwealth realm Crown government in the course of their duties.

Live Templates of a Supramolecular Block Copolymer for the Synthesis of Ordered Nanostructured TiO_2 Films via Guest Exchange

*Wei-Tsung Chuang,**† *Yan-Ming Hsu,*‡ *En-Li Lin,*# *I-Ming Lin,*# *Ya-Sen Sun,**‡ *Yeo-Wan Chiang,*# *Chun-Jen Su,*† *Yao-Chang Lee,*† *U-Ser Jeng*†,§

†National Synchrotron Radiation Research Center, Hsinchu, 30076, Taiwan.

‡Department of Chemical and Materials Engineering, National Central University, Taoyuan 32001, Taiwan.

#Department of Materials and Optoelectronic Science, Center for Nanoscience and Nanotechnology, National Sun Yat-Sen University, Kaohsiung 80424, Taiwan.

§ Department of Chemical Engineering, National Tsing Hua University, Hsinchu 30013, Taiwan

KEYWORDS: block copolymers, mesoporous films, vertical channels, dendrons, guest exchange.

ABSTRACT. In this work, we introduce a facile method based on host–guest chemistry to synthesize a range of nanostructured TiO_2 materials using supramolecular templates of a

dendron-jacketed block copolymer (DJBCP). The DJBCP is composed of amphiphilic dendrons (4'-(3,4,5-tridodecyloxybenzoyloxy)benzoic acid, TDB) selectively incorporated into a P4VP block of polystyrene-*block*-poly(4-vinylpyridine) (PS-*b*-P4VP) via hydrogen bonding. The PS-*b*-P4VP host acts as a structure-directing template, while the guest molecules (TDB) assist the self-assembly nanostructures and zone-axis alignment, resulting in the nanostructured template of vertically oriented cylinders formed via successive phase transformations from $Im\bar{3}m$ to $R\bar{3}m$ to *P6mm* upon thermal annealing in the doctor-blade-cast film. The guest molecules subsequently direct the titania precursors into the P4VP domains of the templates via supramolecular guest exchange during immersion of the film in a designated precursor solution containing a P4VP-selective solvent. The subsequent UV irradiation step leads to the formation of PS-*b*-P4VP/TiO_2 hybrids. Finally, removal of the host template by calcination leaves behind mesoporous channels and makes sacrifices to be a carbon source for carbon-doping TiO_2 materials. Various TiO_2 nanoarchitectures, namely, vertical and wiggly micrometer-length channels, inverse opals, fingerprint-like channels, heterogeneous multilayers, and nanotubes, have been fabricated by highly tunable DJBCP nanostructures.

INTRODUCTION

Ordered mesoporous metallic /or metal oxide films have stimulated great interest in fundamental research into these materials and in their engineering applications such as photovoltaics, catalysis, sensing, separation, and sustainable energy generation.[1–10] One-dimensional (1D) TiO_2 nanochannels enhance charge transport and markedly improve the charge collection efficiency in applications of nanostructured photocatalysts[1–6] by providing a continuous pathway along which photogenerated electrons travel. This pathway results in far

fewer grain boundaries, thus preventing great loss of charge due to recombination. Unfortunately, the 1D nanostructured photoelectrode has a surface area smaller than that of disordered networks of nanoparticles. Therefore, it is desirable to develop a straightforward strategy that increases the surface area per unit volume of channels while preserving their directionality and continuity. Some investigators have fabricated helical inorganic mesoporous fibers with a high channel path[11, 12] or helical pillars[13] by using chiral soft templates, while others have synthesized two-dimensional (2D) arrays of helical inorganic pillars by glancing-angle deposition.[14–17] The fabrication of vertically oriented mesoporous metallic /or metal oxide films with helical nanochannels via a bottom-up approach, however, remains a challenge and warrants further research. Therefore, it is highly desirable to develop a facile approach to the synthesis of mesoporous films with high-surface-area vertical channels.

Amphiphilic surfactants, low-molecular-weight triblock copolymers (P123 and F127, for example), or a combination of both are typically incorporated into metal oxide precursors to assemble structural colloids and thus form hybrid templates for mesoporous metal oxide materials with nanosized pores through sol–gel synthesis[18–20] or evaporation-induced self-assembly.[21, 22] These co-assembly templates generally produce mesoporous metal oxide powders without preferential pore orientation. Several groups have developed unique approaches employing micelle-template syntheses to fabricate mesoporous metal oxide films containing vertical channels.[23–27] These mesoporous films, however, are limited to small pore sizes and short transmission channels, and require specific substrates.

The capabilities of self-assembled films of neat block copolymers (BCPs) in controlling the local ordering and structural orientation, as well as their amenability to selective etching of eligible blocks, render their nanostructures and their high film-forming property particularly

attractive, especially in applications requiring templates for mesoporous materials with tunable pore sizes.[28, 29] BCP thin films forming vertical cylinders have been prepared by using different approaches involving modified substrate surfaces,[30, 31] external fields,[32–34] microwave annealing,[35, 36] solvent annealing and evaporation,[37–45] thermal annealing,[46] and side-chain liquid crystals.[47–52] These highly ordered, vertically oriented cylinder-forming templates have been largely employed in the fabrication of 2D metal oxide pillar arrays using the common etching-and-backfilling method.[53–55] However, production of mesoporous metallic /or metal oxide materials rarely use the BCP templates because the ordered cylinders often collapse after pore wall etching (major-phase microdomains of BCP). Therefore, new fabrication strategies that utilize templates for cylinder-forming BCP films, which retain the micrometer length of their vertical channels even after metal or oxide implantation, are urgent and need to be developed.

Morphological control using supramolecular dendron-jacketed block copolymers (DJBCPs) in a side-chain liquid-crystalline (LC) phase has given rise to many fascinating hierarchical structures such as hexagonally shaped cylinders, ultra-asymmetric lamellae, and tetragonally perforated layers (TPL).[56–58] Such hierarchically ordered DJBCP nanodomains are very appealing candidates for use as nanotemplates, especially for fabricating metal oxide mesoporous materials for vertically oriented channels; the adjustable and thermally stable LC phases of dendron-jacketed blocks can facilitate long-range ordering of phase-separated nanodomains up to the centimeter-length scale.

In this work, we introduce a facile and powerful method of DJBCP-templated synthesis that is able to form various TiO_2 nanoarchitectures via guest exchange. The supramolecular PS-*b*-P4VP(TDB)$_x$ complex with modulated TDB grafting density (x) was used for DJBCP templates. These highly tunable nanostructures of DJBCP templates for fabricating various TiO_2

nanoarchitectures through guest exchange are termed "live" templates. Using by grazing-incidence small-angle X-ray scattering (GISAXS), transmission electron microscopy (TEM), and atomic force microscopy (AFM), we demonstrated the fabrication of vertically oriented micrometer-length cylinders, via successive phase transitions, in a doctor-blade casting DJBCP film. By employing the guest-exchange strategy in place of the conventional etching-and-backfilling method, we preserved the TiO_2 walls and vertical channels formed by DJBCP-templated synthesis. By introducing specially designed and effort-saving UV irradiation and calcination steps, we produced wiggly carbon-doped channels with increased surface area per volume in the vertically oriented mesoporous TiO_2 film. Understanding the mechanism of guest exchange enabled us to construct the desired TiO_2 nanostructures via live templates of DJBCP superstructures. Using the technique presented in this study, we synthesized not only mesoporous TiO_2 films with fingerprint, inverse opal, and heterogeneous multilayer structures, but also TiO_2 nanotubes.

Results and discussion

DJBCP-templated synthesis with guest exchange. Figure 1 depicts a representative four-step process used to fabricate vertically oriented mesoporous TiO_2 films with wiggly channels. In the first step (*i*), the PS-*b*-P4VP(TDB)$_{0.7}$ film with vertically oriented cylinders can be prepared by doctor-blade casting followed by thermal annealing at 150 °C, which is discussed in a later section. In the second step (*ii*), the DJBCP templates are immersed in a 0.15 M TiF_4 solution in ethanol (P4VP-selective solvent) for 1–2 h in order to replace the hydrogen-bonded dendrons with titanium ions, which exhibit stronger coordinate bonding. The insoluble PS domains with high glass-transition temperature (ca. 100 °C) can thus retain their original morphology, while

the guest molecules of TDB dendrons serve as both site- and structure holders that guide the TiO_2 precursors during the swelling of P4VP domains.

In the third step (*iii*), the PS-*b*-P4VP/TiO_2 precursor host–guest hybrid is exposed to UV radiation using a mercury lamp under controlled relative humidity (ca. 65~70 %). This step produces TiO_2 from TiF_4 by hydrolysis. The UV radiation not only provides a moderate and uniform temperature gradient (ca. 65 °C) for TiO_2 synthesis but also aids cross-linking of the PS domains for further carbonization.[59–62] With depending on film thickness, we adjusted appropriately the distance between sample and mercury lamp around 10~15 cm and exposure time around 8~12 h in order to slow down the hydrolysis rate and to avoid decomposition of block copolymers by excessive exposure of UV radiation.[10] In the last step (*iv*), the PS-*b*-P4VP host is removed from the PS-*b*-P4VP/TiO_2 hybrid by calcination at 500 °C to yield a vertically oriented mesoporous anatase TiO_2 matrix with wiggly and open channels.

Film contraction after calcination enables formation of wiggly channels with increased surface area per unit volume without resorting to expensive procedures. By employing different nanostructured DJBCP films, this method can be used to synthesize various TiO_2 nanostructures, which is demonstrated in the latest section.

Mesoporous TiO_2 film with vertical and wiggly channels. Shown in Figure 2 are the GISAXS patterns and in-plane scattering profiles for the structural evolution of the DJBCP-template during the four-step synthesis as illustrated in Figure 1. The GISAXS pattern for the as-cast film after the thermal annealing (step (*i*), Figure 2a) displays a series of reflection spots in the low-q region along the q_y direction; its ratio between peak positions and the first peak position (q/q^*) have 1:√3:2:√7:3 (Figure 2b(*i*)), corresponding to a hexagonal arrangement with lattice parameter a of 36.7 nm. Ring-like reflections in Figure 2a(*i*) with a peak-position ratio of

1:2 in the high-q region were identified as (01) and (02) reflections of a smectic LC phase consisting of dendron-jacketed blocks P4VP(TDB)$_{0.7}$. These observations indicate that the thin-film morphology of PS-*b*-P4VP(TDB)$_{0.7}$ exhibits a hierarchical structure of HEX_{CYL} within a smectic LC phase, in which the cylinders are perpendicular to the substrate. Since the volume fraction of PS (ϕ_{PS}) is 0.29 in the case of PS-*b*-P4VP(TDB)$_{0.7}$, the cylinder microdomains were composed of PS blocks.

In step (*ii*), the broadening scattering peaks of the HEX_{CYL} structure factor (Figure 2b(*ii*)) can be attributed to precursor solution adsorption onto the film after immersion. The absence of smectic signals in the high-q region (Figure 2a(*ii*)) signifies that the new host–guest complex of P4VP–titanium ions with stronger ionic bonding replaced the hydrogen-bonding complexes of the dendrons after immersion in the precursor solution. FTIR spectral analysis also confirmed the formation of new host–guest complexes between P4VP and titanium ions via supramolecular guest exchange after immersion in the precursor solution. The FTIR spectra in Figure 3 reveals the emergence of a new metal-bonded CN stretching mode at 1637 cm^{-1} due to coordination of pyridyl groups of P4VP chains with titanium ions, as well as the disappearance of the hydrogen-bonded lines of the P4VP(TDB)$_{0.7}$ complexes at 1607 and 1014 cm^{-1}.

Strengthening of the HEX_{CYL} scattering peaks after hydrolysis of the complex (Figure 2b(*iii*)) indicates that UV irradiation did not affect the cylinder orientation and hexagonal ordering. Moreover, the lattice parameter a (40.3 nm) extracted from the primary (100) reflection of HEX_{CYL} is ca. 10 % greater than its original value of 36.7 nm. This is presumably due to post-hydrolysis expansion of the spacing between PS cylinder domains.

Finally, calcination at 500 °C for 3 h led to the formation of crystalline anatase, as shown by the XRD profile in Figure S1. The removal of PS-*b*-P4VP left behind deformed channels in the

mesoporous TiO_2 film, as suggested by the decreasing number of scattering peaks for HEX_{CYL} in Figure 2b(iv). The corresponding SEM image of the 1 μm thick mesoporous TiO_2 film in Figure 4a confirms the distribution of vertically oriented wiggly nanochannels over a wide cross-section of the film. The top-view SEM image in Figure 4b displays a locally hexagonal arrangement of pores, wide pore openings, and a narrow pore size distribution at ca. 18 nm. The formation of wiggly channels may be attributed to unidirectional film contraction along the film normal. Before calcination, the P4VP blocks, which correspond to a P4VP volume fraction (ϕ_{P4VP}) of around 0.11, acted as scaffolds within the amorphous TiO_2 grains that held the pore walls of the template. Decomposition of P4VP blocks during calcination left residual spaces within the pore walls. Therefore, TiO_2 grain rearrangement by crystallization forming rigid pore walls induced film contraction and formation of vertically oriented wiggly channels upon removal of the cylindrical PS domains.

Film contraction in the DJBCP-templated synthesis unexpectedly produced wiggly channels with a surface area per unit volume larger than that of straight channels. We also prepared mesoporous TiO_2 films with vertically oriented wiggly channels of ca. 400 nm thickness by varying the concentration of the DJBCP solution (Figure 4c). The result indicates that the length of vertical TiO_2 channels can be controlled in the DJBCP-templated synthesis.

We opted to use UV irradiation for TiO_2 reduction instead of conventional thermal treatment at 65 °C in order to maintain a lower reaction rate. Conventional thermal treatment leads to rapid and uncontrolled hydrolysis, which, in turn, causes dense TiO_2 precipitation on the surface, sealing the channel pores after calcination (Figure S2). The UV irradiation step also provides an additional benefit of cross-linked PS-*b*-P4VP for carbonization after calcination. The characteristic G and D lines (ca. 1600 cm^{-1} and ca. 1350 cm^{-1}, respectively) in the Raman

spectrum for the hybrid mesoporous film with carbon-coated TiO_2 nanochannels further reveals the graphitic nature of the film (Figure S3a). A characteristic carbon peak in the EDS spectrum (Figure S3b) also implies that residual carbon from the calcination of the copolymer accumulated on the walls of mesoporous TiO_2 anatase. The presence of partially graphitic carbons may be due to the carbonization of possibly cross-linked PS-*b*-P4VP under UV radiation at 500 °C during calcination.[59–62] Such carbonization facilitates the formation of rigid confinement walls during channel formation, resulting in the ordered channel structure after calcination.[59] The presence of partially graphitic carbons in mesoporous TiO_2 could markedly enhance electron collection and increase electrical conductivity in highly efficient dye-sensitized solar cells reported by Jang et al..[62]

Formation of DJBCP template of vertically oriented cylinders. Single zone-axis alignment with order–order phase transitions plays a critical role in the formation of the DJBCP films with vertically oriented cylinder. Using ex situ GISAXS, TEM, and AFM measurements, we tracked the structural evolution of doctor-blade-cast films during annealing at 150 °C (results are shown in Figures 5 and S4). In the cross-sectional TEM image shown in Figure 5a, the bright zones aligned along the film normal correspond to PS domains. In addition, a six-fold packing symmetry of the film surface shown in the AFM image in Figure S4a reveals that the morphology of the as-cast film before annealing took the form of cube-like packed spheres. The corresponding GISAXS pattern in Figure 5b reveals two diffraction spots lacking high-order symmetry, which are assigned as $(1\,\bar{1}\,0)$ and (110) reflections according to an $Im\bar{3}m$ mesostructure with a = 39.2 nm. These findings demonstrate that the <111> direction of the $Im\bar{3}m$ mesostructure is perpendicular to the substrate, in contrast to the common <110>-oriented $Im\bar{3}m$ spheres in thick films of neat BCP systems.[64–66]

We found that the $(1\bar{1}0)$ and (110) reflections in the GISAXS patterns remained unchanged despite rotation of the as-cast film. We also performed fast Fourier transform (FFT) analysis on two representative zones from the cross-sectional TEM images in Figure 5a. The two FFT patterns presented in Figure S5 may be regarded as being viewed from the <121> and <022> zone axes of the <111>-aligned $Im\bar{3}m$ mesostructure. These results indicate that the as-cast film of the <111>-aligned $Im\bar{3}m$ mesostructure is polycrystalline and that uniaxial rotation occurs along the <111> zone axis, which is parallel to the film normal. Ordered structures with a perfect single-crystal arrangement are not required in the formation of vertical cylinders in our method, as long as the <111> direction of the $Im\bar{3}m$ mesograins can be aligned perpendicular to the substrate.

Upon inspection of Figure 5a, we found that the PS spheres exhibited a slightly elliptical shape with its major axis preferentially aligned parallel to the film normal (or perpendicular to the shear direction). That is, the preferred deformation direction of PS globular domains is perpendicular to the shear direction. As demonstrated in our previous work,[57] such behavior results from the greater chain mobility of the supercooled smectic LC domains of dendron-jacketed blocks compared with that of PS domains. Both the uniaxial deformation of spheres along the <111> direction and the preferential <111> orientation of $Im\bar{3}m$ spheres are kinetically triggered by the parallel-oriented smectic LC layers under the casting processes (Figure S6). Both provide a shortcut for epitaxial growth for HEX_{CYL} (*P6mm*) through the fusion of spheres along the <111> direction of the $Im\bar{3}m$ structure.[67]

Upon annealing at 150 °C for 2 h, the partial spheres transformed into short cylinders. The coexistence of both morphologies is visible in the cross-sectional TEM image in Figure 5c. In the corresponding GISAXS pattern (Figures 5d and S7), an in-plane reflection at q = 0.2 nm^{-1} is

assigned to the $(100)_{P6mm}$ plane of the HEX_{CYL} mesostructure with a = 36.3 nm. The deduced lattice size is consistent with the average distance of nearest-neighbor cylinders of ca. 37 nm, as obtained from the TEM image in Figure 5c. Other corresponding reflections are indexed to (100), (110), and (111) for a rhombohedral mesostructure ($R\bar{3}m$) with a = 39.3 nm and lattice angle (α) of 116°, different from that of $Im\bar{3}m$. This intermediate $R\bar{3}m$ mesostructure reveals traces of the unidirectional contraction of the $Im\bar{3}m$ lattice along the <111> direction, the film normal, under thermal annealing. Along with the unidirectional contraction accompanying the $Im\bar{3}m$-to-$R\bar{3}m$ transition, the d spacing of the (111) plane decreased from 22.6 nm ($d_{111}^{Im\bar{3}m}$) to 19.3 nm ($d_{111}^{R\bar{3}m}$; a decrease of ca. 37 %), corresponding to a ~40 % decrease in film thickness as estimated by AFM. In addition, α increased from 90° to 116° during the transition. In Figure 5c, the nucleation of HEX_{CYL} grains strongly suggests that the neighboring spheres merged along the <111> direction of the intermediate $R\bar{3}m$ mesostructure (film normal). The in-plane growth of the short-cylinder grains presumably gave rise to the lamellae-like architectures of HEX_{CYL}, which were distributed not only near the top surface but also within the interior of the film. This process is largely different from that occurring in solvent annealing, whereby the cylinder nucleation sites originate at the top surface of neat BCP thin films because of rapid solvent evaporation.[37–39]

After further annealing for 15 h, the reflections of the $R\bar{3}m$ phase disappeared, while the in-plane reflections gradually developed into high-order reflections that can be assigned to (100), (110), (200), and (210) reflections of HEX_{CYL} (Figures 5f and S7). The cross-sectional TEM image in Figure 5e demonstrates that the HEX_{CYL} grains coarsened and the vertical cylinders increased in length (via merging) gradually throughout the entire film thickness. The longer annealing time ensured that the HEX_{CYL} grain boundaries were completely eliminated to allow the channels to reach micrometer length. We observe that the mesophase between the sphere and

cylinder phases is strongly dependent on the preferential orientation of the lattice plane relative to the substrate in its initial state. For instance, <110>-oriented $Im\bar{3}m$ spheres formed HEX_{CYL} (*P6mm*) via intermediate *Fmmm* spheres.[47] Therefore, determining the correct pathway from many diverging kinetic routes is vital to preparing vertically oriented cylinders via epitaxial growth. With similar kinetic-route control in our previous work, we also observed a subtle transition from the distorted spheres with face-centered-cubic packing to TPL via an epitaxial extension along the <110> direction under thermal stretching.[56, 57]

Various TiO_2 nanostructures from live templates of DJBCP. The key step to fabricating robust mesoporous TiO_2 films lies in the delicate pathway of DJBCP-templated synthesis, which facilitates supramolecular guest exchange and directs the incorporation of the TiO_2 precursor into the specific domains of the superstructured BCP templates. Specifically, the supramolecular dendrons hold the binding sites and strengthen the superstructured BCP templates, hence enabling site-specific exchange with the precursor within the rigid template structures. The dendrons occupied a large volume fraction (ϕ_{TDB}), ca. 0.6 and 0.52 in PS-*b*-P4VP(TDB)$_x$ with x values of 0.7 and 0.5, respectively. The removal of TDB dendrons upon immersion in the precursor solution releases a large volume of space that allows titania precursors to significantly penetrate the P4VP-host domains, thus leading to a sturdy TiO_2 matrix. The morphology of the insoluble PS domains determines the porous form of the mesoporous TiO_2 films. Therefore, DJBCP-templated synthesis coupled with guest exchange can efficiently incorporate titania into the host microdomains of the templates in the construction of various ordered TiO_2 nanostructures.

To verify the applicability of this method to other nanostructured DJBCP templates, we prepared two DJBCP templates from as-cast films of PS-*b*-P4VP(TDB)$_x$ with x = 0.7 and 0.5 that

have the ordered morphologies of cubic packed spheres and typically parallel cylinders, respectively (Figure S8). These templates were used to synthesize inverse opal-like TiO_2 nanostructures and fingerprint-like TiO_2 channels, which are shown in Figures 6a and 6b, respectively.

Since the zone-axis alignment with phase transformations that governs the formation of vertically oriented cylinders have a minimal interfacial effect on substrates in the DJBCP film, layer-by-layer doctor-blade casting process can form mesoporous TiO_2 films with the stacked-layer nanoarchitecture having heterogeneous multilayers. Figure 6c presents the fabricated nanochannel-on-nanoparticle TiO_2 multilayer structure, in which the mesoporous layer of vertical nanochannels was formed by DJBCP-template synthesis, and the underlying nanoparticle layer was derived from commercially available P-25 TiO_2 nanoparticles. These three-dimensional ordered TiO_2 nanoarchitectures with varying configurations of mesoporous TiO_2 layers are promising frameworks for photoelectrodes, since they could enhance electron transport and provide a large surface area that increases accessibility of chemical reaction sites as demonstrated by Villanueva-Cab et al..[68]

In addition to fabricating nanostructured mesoporous TiO_2 films, we employed the guest-exchange method to synthesize individual TiO_2 nanotubes using a DJBCP nanopillar template. We prepared individual PS-core@P4VP-shell pillars by immersing a PS-*b*-P4VP(TDB)$_{0.7}$ film of vertically oriented cylinders in excess cold ethanol. This technique freezes the dynamics of the PS-core domains and, in turn, leads to the removal of TDB. The pillars on sticking together (as representatively shown in Figure 7a) are due to immersion without stir and short immersing time in order to take the sample conveniently for the SEM experiment. The presence of pillars (ca. 30 nm diameter) after TDB removal implies that the PS-core domains of dispersed pillars retain

their form during ethanol immersion and that the dissolved P4VP chains constitute the hairy-like shell.[69-71] Hence, the guest-exchanged Ti precursors can be distributed uniformly within the guiding P4VP shell domains of the pillars upon immersion of the pillars in 5 wt % precursor/ethanol solution. A 2:1 mixture of 1,5-pentanediol and titanium(IV) tetrabutoxide was used as the TiO_2 precursor. The precursor can be subsequently reduced to amorphous TiO_2 by adding deionized water at 80 °C to a pressure tube to produce the BCP/TiO_2 pillar hybrids. The pillar hybrids were then separated by centrifugation. Finally, we removed PS-*b*-P4VP by calcination at 500 °C, which yielded curved and fragile anatase TiO_2 nanotubes with open ends, as shown in Figure 7b. The pore diameter of the resultant nanotubes is ca. 15 nm, which corresponds to the original size of the PS core. Furthermore, the walls of the TiO_2 nanotubes are approximately 30 nm thick, which is about twice as thick as the P4VP shell of the BCP pillars. This indicates that the growth of the TiO_2 nanotube wall is not limited by the core–shell template in the precursor solution.

CONCLUSION

In summary, we have demonstrated that DJBCP-templated synthesis coupled with guest exchange is a simple method of synthesizing nanostructured TiO_2 materials having structures such as vertical and wiggly micrometer-length channels, fingerprint structures, inverse opals, and nanotubes. By elucidating the mechanism of guest exchange, we were able to fabricate the desired TiO_2 architectures using live templates of DJBCP superstructures. The mechanism of order–order phase transitions ensured that the formation of vertically oriented cylinders is no longer limited to specific substrates. The highly versatile cylinder-forming films can be used to generate mesoporous TiO_2 multilayers containing channels of specific orientations. The

dissolution of the cylinder-forming DJBCP film in a P4VP-selective solvent enabled the isolation of individual PS-core@P4VP-shell pillars surrounded by a shell consisting of covalently bound P4VP chains. These manostructured TiO_2 materials have potential use in important applications such as those in electrodes, sensors, optoelectronic devices, and catalysts. Supramolecular BCP-templated synthesis coupled with guest exchange opens the possibility of tailoring the shape, length, and orientation of mesopores for other mesoporous metallic /or metal oxide materials.

EXPERIMENTAL SECTION

Materials and sample preparation. We prepared dendrons of 4'-(3,4,5-tridodecyloxybenzoyloxy)benzoic acid (TDB) according to procedures with modifications.[56] We obtained the diblock copolymer polystyrene-*block*-poly(4-vinylpyridine) (PS-*b*-P4VP) from Polymer Source Inc. The weight-average molecular weights of the blocks are 24 and 9.5 kDa respectively, and the polydispersity index is 1.1. Blend films of PS-*b*-P4VP and TDB (PS-*b*-P4VP(TDB)$_x$) with grafting ratios (x) of 0.7 and 0.5 were cast from *o*-xylene solutions. The films (ca. 400 nm and 1 μm) were prepared by the doctor-blade-cast method (40 and 50 wt % DJBCP/*o*-xylene solutions, respectively). The nanostructures of the films were tuned by varying x or by thermal annealing.[56-58] Table S1 lists the DJBCP morphologies of doctor-blade-cast films with and without thermal annealing at 150 °C for 15 h while varying the volume fraction of PS (ϕ_{PS}) according to x for TDB. For example, the as-cast DJBCP film with x = 0.7 exhibited a spherical morphology, which rearranged into vertically oriented hexagonally packed cylinders (HEX_{CYL}) through a series of order–order phase transitions upon thermal annealing. In contrast, the morphology of the as-cast DJBCP film with x = 0.5 exhibited parallel cylinders resembling a fingerprint pattern. We calculated the volume fractions of PS, P4VP, and TDB from the densities

of PS (1.047 g/cm^3), P4VP (1.114 g/cm^3), and TDB (1.048 g/cm^3), as determined by automatic gas displacement pycnometry. We prepared two separate precursor solutions to synthesize mesoporous TiO_2 films and TiO_2 nanotubes via thermal hydrolysis. For the mesoporous TiO_2 films, we prepared a 1.5 M precursor solution containing titanium tetrafluoride (TiF_4) and the P4VP-selective solvent, ethanol (Sigma-Aldrich). Notably, the reaction to prepare TiO_2 from TiF_4 generates a small amount of hydrogen fluoride (HF), which is a corrosive chemical etchant. For the synthesis of TiO_2 nanotubes, we prepared a second precursor, containing a 2:1 mixture of 1,5-pentanediol and titanium(IV) tetrabutoxide, in ethanol.

Microscopy. We monitored the surface and cross-sectional morphologies of mesoporous TiO_2 films by field-emission scanning electron microscopy (SEM; JEOL JSM-6500F, operated at 10 kV). SEM was performed along with energy-dispersive X-ray spectroscopy (EDS), which was used for elemental analysis. We examined the surface morphologies of DJBCP films using AFM (SPA400 Seiko) in tapping mode. To obtain a cross-sectional image of the copolymer films, we embedded the DJBCP films in epoxy after we coated the films with a carbon layer. The films were subsequently transferred from the substrate onto the epoxy surface after the samples were dipped in liquid nitrogen. The embedded specimens were sectioned with an ultramicrotome (Leica Reichert Ultracut-E). Sections approximately 100 nm thick were placed on a copper grid and stained with iodine vapor for around 8 h for enhanced contrast. The specimens were then imaged by TEM (JEOL TEM 2100, operated at 160 kV). Upon preferential staining with iodine vapor, P4VP microdomains appeared dark whereas PS microdomains appeared bright.

GISAXS and X-ray powder diffraction. We performed GISAXS and X-ray powder diffraction (XRD) at the end stations of the BL23A SWAXS and BL01C2 XRD beamlines, respectively, of the Taiwan Light Source at the National Synchrotron Radiation Research Center

(NSRRC). GISAXS data were obtained from X-rays (15 keV energy, 0.8265 Å wavelength) at an incident angle of 0.2°. All GISAXS data were collected with an area detector (Pilatus 1M-F) that was rigorously corrected for electronic noise, sample transmission, background scattering, and detector sensitivity. We calibrated the area detector for absolute scattering intensity by using a sample of high-density polyethylene, and with silver behenate for the scattering wavevector (q, defined by $4\pi\lambda^{-1}\sin\theta$ and the scattering angle 2θ).[72] In-plane scattering profiles were integrated line cuts along the direction q_y at $q_z \approx 0$ nm^{-1} from the corresponding GISAXS patterns.

FTIR and Raman spectroscopy. Synchrotron FTIR spectroscopy measurements were performed at the end stations of the BL14A beamline of the Taiwan Light Source at NSRRC. We recorded Raman spectra using a Raman microscope spectrometer operated at an excitation wavelength of 633 nm.

ASSOCIATED CONTENT

Supporting Information. Full details of GISAXS data, AFM, SEM images and Ramman spectrum. The Supporting Information is available free of charge on the ACS Publications website at DOI: XXXXX .

AUTHOR INFORMATION

Corresponding Author

* E-mail: weitsung@nsrrc.org.tw

* E-mail: yssun@cc.ncu.edu.tw

ACKNOWLEDGMENT

Financial support from the Ministry of Science and Technology, Taiwan (MOST 104-2628-E-213 -001 -MY3) is gratefully acknowledged.

REFERENCES

(1) Chen, X.; Mao, S. S. Titanium Dioxide Nanomaterials: Synthesis, Properties, Modifications, and Applications. *Chem. Rev*. **2007**, *107*, 2891-2959.

(2) Fattakhova-Rohlfing, D.; Zaleska, A.; Bein, T. Three-Dimensional Titanium Dioxide Nanomaterials. *Chem. Rev*. **2014**, *114*, 9487-9558.

(3) Li, W.; Wu, Z; Wang, J.; Elzatahry, A. A.; Zhao, D. Y. A Perspective on Mesoporous TiO_2 Materials. *Chem. Mater.*, **2014**, *26*, 287-298.

(4) Crossland, E. J. W.; Kamperman, M.; Nedelcu, M.; Ducati, C.; Wiesner, U.; Smilgies, D. M.; Toombes, G. E. S.; Hillmyer, M. A.; Ludwigs, S.; Steiner, U.; Snaith, H. J. Block Copolymer Morphologies in Dye-Sensitized Solar Cells: Probing the Photovoltaic Structure−Function Relation. *Nano Lett.* **2009***, 9*, 2813-2819.

(5) Ye, M.; Gong, J.; Lai, Y.; Lin, C.; Lin, Z. High-Efficiency Photoelectrocatalytic Hydrogen Generation Enabled by Palladium Quantum Dots-sensitized TiO_2 Nanotube Arrays. *J. Am. Chem. Soc.*, **2012**, *34*, 15720-15723.

(6) Wang, M.; Zheng, D.; Ye, M.; Zhang, C.; Xu, B.; Lin, C.; Sun, L.; Lin, Z. One-Dimensional Densely Aligned Perovskite-Decorated Semiconductor Heterojunctions with Enhanced Photocatalytic Activity. *Small*, **2015**, *11*, 1436-1442.

(7) Wan, Y.; Yang, H. F.; Zhao, D. Y. "Host-Guest" Chemistry in the Synthesis of Ordered Nonsiliceous Mesoporous Materials. *Acc. Chem. Res.* **2006**, *39*, 423-432.

(8) Vukovic, I.; Punzhin, S.; Vukovic, Z.; Onck, P.; De Hosson, J. T, M.; Brinke, G.; Loos, K. Supramolecular Route to Well-Ordered Metal Nanofoams. *ACS Nano* **2011***, 5*, 6339-6348.

(9) Rawolle, M.; Ruderer, M. A.; Prams, S. M.; Zhong, Q.; Magerl, D.; Perlich, J.; Roth, S. V.; Lellig, P.; Gutmann, J. S.; Müller-Buschbaum, P. Nanostructuring of Titania Thin Films by a Combination of Microfluidics and Block-Copolymer-Based Sol–Gel Templating. *Small*, **2011**, *7*, 884-891.

(10) Song, L.; Abdelsamie, A.; Schaffer, C. J.; Körstgens, V.; Wang, W.; Wang, T.; Indari, E. D.; Fröschl, T.; Hüsing, N.; Haeberle, T.; Lugli, P.; Bernstorff, S.; Müller-Buschbaum, P. A Low Temperature Route toward Hierarchically Structured Titania Films for Thin Hybrid Solar Cells *Adv. Funct. Mater.* **2016**, *26*, 7084-7093.

(11) Li, Y.; Bi, L.; Wang, S.; Chen, Y.; Li, B.; Zhu, X.; Yang, Y. Preparation of Helical Mesoporous Ethylene–Silica Nanofibers with Lamellar Mesopores on the Surfaces. *Chem. Commun.* **2010***, 46*, 2680-2682.

(12) Xie, J.; Duan, Y.; Che, S. Chirality of Metal Nanoparticles in Chiral Mesoporous Silica. *Adv. Funct. Mater.* **2012***, 22*, 3784-3792.

(13)Tseng, W. H.; Chen, C. K.; Chiang, Y. W.; Ho, R. M.; Akasaka, S.; Hasegawa, H. Helical Nanocomposites from Chiral Block Copolymer Templates. *J. Chem. Am. Soc.* **2009**, *131*, 1356-1357.

(14) Ye, D. X.; Karabacak, T.; Picu, R. C.; Wang, G. C.; Lu, T. M. Uniform Si Nanostructures Grown by Oblique Angle Deposition with Substrate Swing Rotation. *Nanotechnology,* **2005***, 16,* 1717-1723.

(15) van Popta, A. C.; Brett, M. J.; Sit, J. C. Double-Handed Circular Bragg Phenomena in Polygonal Helix Thin Films. *J. Appl. Phys.,* **2005***, 98*, 083517

(16) Krause, K. M.; Brett, M. J. Spatially Graded Nanostructured Chiral Films as Tunable Circular Polarizers. *Adv. Funct. Mater.,* **2008***, 18*, 3111-3118.

(17) Huang, Z. F.; Harris, K. D.; Brett, M. J. Morphology Control of Nanotube Arrays. *Adv. Mater.,* **2009***, 21*, 2983-2987.

(18) Kresge, C. T.; Leonowicz, M. E.; Roth, W. J.; Vartuli, J. C.; Beck, J. S. Ordered Mesoporous Molecular Sieves Synthesized by a Liquid-Crystal Template Mechanism. *Nature*, **1992**, 359 710-712.

(19) Antonelli, D. M.; Ying, J. Y. Synthesis of Hexagonally Packed Mesoporous TiO_2 by a Modified Sol–Gel Method. *Angew. Chem. Int. Ed.* **1995**, 34, 2014-2017.

(20) Antonelli, D. M. Synthesis of Phosphorus-free Mesoporous Titania via Templating with Amine Surfactants. *Micropor. Mesopor. Mater* **1999**, 30, 315-319.

(21) Yang, P. D.; Zhao, D. Y.; Margolese, D. I.; Chmelka, B. F.; Stucky, G. D. Generalized Syntheses of Large-Pore Mesoporous Metal Oxides with Semicrystalline Frameworks. *Nature*, **1998**, *396*, 152-155.

(22) Brinker, C. J.; Lu, Y. F.; Sellinger, A.; Fan, H. Y. Evaporation-induced Self-assembly: Nanostructures Made Easy. *Adv. Mater.* **1999**, *11*, 579-585.

(23) Shan, F.; Lu, X.; Zhang, Q.; Wu, J.; Wang, Y.; Bian, F.; Lu, Q.; Fei, Z.; Dyson, P. A Facile Approach for Controlling the Orientation of One-Dimensional Mesochannels in Mesoporous Titania Films. *J. Am. Chem. Soc.* **2012**, *134*, 20238-20241.

(24) Koh, C. W.; Lee, U. H.; Song, J. K.; Lee, H. R.; Kim, M. H.; Suh, M.; Kwon, Y. U. Mesoporous Titania Thin Film with Highly Ordered and Fully Accessible Vertical Pores and Crystalline Walls. *Chem. Asian J.* **2008**, *3*, 862-867.

(25) Richman, E. K.; Brezesinski, T.; Tolbert, S. H. Vertically Oriented Hexagonal Mesoporous Films Formed through Nanometre-Scale Epitaxy. *Nat. Mater.* **2008**, *7*, 712-717.

(26) Kao, K. C.; Lin, C. H.; Chen, T. Y.; Liu, Y. H.; Mou, C. Y. A General Method for Growing Large Area Mesoporous Silica Thin Films on Flat Substrates with Perpendicular Nanochannels. *J. Am. Chem. Soc.* **2015**, *137*, 3779-3782.

(27) Ko, Y. S.; Koh, C. W.; Lee, U. H.; Know, Y. K. Synthesis of Mesoporous Titania Thin Films with Vertical Pore Channels and Thick and Crystalline Walls. *Micropor. Mesopor. Mater* **2011**, *145*, 141-145.

(28) Orilall, M. C.; Wiesner, U. Block Copolymer Based Composition and Morphology Control in Nanostructured Hybrid Materials for Energy Conversion and Storage: Solar Cells, Batteries, and Fuel Cells. *Chem. Soc. Rev.* **2011**, *40*, 520-535.

(29) Hur, K.; Wiesner, U. Design and Applications of Multiscale Organic–inorganic Hybrid Materials Derived from Block Copolymer Self-Assembly. *Adv. Polym. Sci.* **2013**, *262*, 259-294.

(30) She, M. S.; Lo, T. Y.; Ho, R. M. Long-Range Ordering of Block Copolymer Cylinders Driven by Combining Thermal Annealing and Substrate Functionalization. *ACS. Nano* **2013**, *7*, 2000-2011.

(31) Han, E.; Stuen, K. O.; Leolukman, M.; Liu, C. C.; Nealey, P. F.; Gopalan, P. Perpendicular Orientation of Domains in Cylinder-Forming Block Copolymer Thick Films by Controlled Interfacial Interactions. *Macromolecules* **2009**, *42*, 4896-4901.

(32) Thurn Albrecht, J. S. T.; Krusin-Elbaum, K. L.; Black, C. T.; Tuominen, M. T.; Russell, T. P. Ultrahigh-density Nanowire Arrays Grown in Self-Assembled Diblock Copolymer Templates. *Science* **2000***, 290*, 2126-2129.

(33) Goldberg-Oppenheimer, P.; Kabra, D.; Vignolini, S.; Hüttner, S.; Sommer, M.; Neumann, K.; Thelakkat, M.; Steiner, U. Hierarchical Orientation of Crystallinity by Block-copolymer Patterning and Alignment in an Electric Field. *Chem. Mater.* **2013**, *25*, 1063-1070.

(34) Tang, C.; Wu, W.; Smilgies, D. M.; Matyjaszewski, K.; Kowalewski, T. Robust Control of Microdomain Orientation in Thin Films of Block Copolymers by Zone Casting. *J. Am. Chem. Soc.* **2011**, *133*, 11802-11809.

(35) Jin, C.; Murphy, J. N.; Harris, K. D.; Buriak, J. M. Deconvoluting the Mechanism of Microwave Annealing of Block Copolymer Thin Films. *ACS Nano* **2014**, *8*, 3979-3991.

(36) Borah, D.; Senthamaraikannan, R.; Rasappa, S.; Kosmala, B.; Holmes, J. D.; Morris, M. A. Swift Nanopattern Formation of PS-*b*-PMMA and PS-*b*-PDMS Block Copolymer Films Using a Microwave Assisted Technique. *ACS Nano* **2013***, 7*, 6583-6596.

(37) Kim, S. H.; Misner, M.; Xu, T.; Kimura, M.; Russell, T. P. Highly Oriented and Ordered Arrays from Block Copolymers via Solvent Evaporation. *Adv. Mater.* **2004**, *16*, 226-231.

(38) Ho, R. M.; Tseng, W. H, a, Fan, H. W.; Chiang, Y. W.; Lin, C. C.; Ko, B. T.; Huang, B. H. Solvent-induced Microdomain Orientation in Polystyrene-*b*-Poly (L-lactide) Diblock Copolymer Thin Films for Nanopatterning. *Polymer* **2005***, 46*, 9362-9377.

(39) Phillip, W. A.; Hillmyer, M. A.; Cussler, E. L. Cylinder Orientation Mechanism in Block Copolymer Thin Films upon Solvent Evaporation. *Macromolecules* **2010***, 43*, 7763-7770.

(40) Peinemann, K.; Aberz, V.; Simon, P. F. W. Asymmetric Superstructure Formed in a Block Copolymer via Phase Separation. *Nat. Mater.* **2007***, 6*, 992-996.

(41) Yin, J.; Yao, X.; Liou, J. Y.; Sun, W.; Sun, Y. S.; Wang, Y. Membranes with Highly Ordered Straight Nanopores by Selective Swelling of Fast Perpendicularly Aligned Block Copolymers. *ACS Nano* **2013***, 7*, 9961-9974.

(42) Gowd, E. B.; Bŏhme, M.; Stamm, M. In Situ GISAXS Study on Solvent Vapour Induced Orientation Switching in PS-*b*-P4VP Block Copolymer Thin Films. *Synchrotron Radiat. Polym. Sci.* **2010**, *14*, 012015.

(43) Park, S.; Wang, J. Y.; Kim, B.; Xu, J.; Russell, T. P. A Simple Route to Highly Oriented and Ordered Nanoporous Block Copolymer Templates. *ACS Nano* **2008***, 2*, 766-772.

(44) Sinturel, C.; Vayer, M.; Morris, M.; Hillmyer, M. A. Solvent Vapor Annealing of Block Polymer Thin Films. *Macromolecules* **2013,** *46*, 5399-5415.

(45) Cui, G.; Fujikawa, M.; Nagano, S.; Shimokita, K.; Miyazaki, T.; Sakurai, S.; Yamamoto, K. Macroscopic Alignment of Cylinders via Directional Coalescence of Spheres Along Annealing Solvent Permeation Directions in Block Copolymer Thick Films. *Macromolecules* **2014**, *47*, 5989-5999.

(46) Sakurai, S.; Bando, H.; Yoshida, H.; Fukuoka, R.; Mouri, M.; Yamamoto K.; Okamoto, S.; Spontaneous Perpendicular Orientation of Cylindrical Microdomains in a Block Copolymer Thick Film. *Macromolecules* **2009***, 42*, 2115-2121.

(47) Yoon, J.; Jung, S. Y.; Ahn, B.; Heo, K.; Jin, S.; Iyoda, T.; Yoshida, H.; Ree, M. Order−Order and Order−Disorder Transitions in Thin Films of an Amphiphilic Liquid Crystalline Diblock Copolymer. *J. Phys. Chem. B* **2008***, 112*, 8486-8495.

(48) Huang, W. H.; Chen, P. Y.; Tung, S. H. Effects of Annealing Solvents on the Morphology of Block Copolymer-Based Supramolecular Thin Films. *Macromolecules* **2012**, *45*, 1562.

(49) Wang, J.; Odarchenko, Y. I.; Defaux, M.; Lejnieks, J.; Ahokhin, D. V.; Keul, H.; Ivanov, D. A.; Möller, M.; Mourran, A. Concurrent Order in a Semi-Crystalline Diblock Copolymer Involving Complexation with a Mesogen. *Macromolecules* **2013**, *46*, 6159-6168.

(50) Komura, M.; Iyoda, T. AFM Cross-sectional Imaging of Perpendicularly Oriented Nanocylinder Structures of Microphase-separated Block Copolymer Films by Crystal-like Cleavage. *Macromolecules* **2007,** *40,* 4106-4108.

(51) Yamamoto, T.; Taro Kimura, T.; Komura, M.; Suzuki, Y.; Iyoda, T.; Asaoka, S.; Nakanishi, H. Block Copolymer Permeable Membrane with Visualized High-density Straight Channels of Poly(ethylene oxide). *Adv. Funct. Mater.* **2011**, *21*, 918-926.

(52) Asaoka, S.; Uekusa, T.; Tokimori, H.; Komura, M.; Iyoda, T.; Yamada, T.; Yoshida, H. Normally Oriented Cylindrical Nanostructures in Amphiphilic PEO–LC Diblock Copolymers Films. *Macromolecules* **2011***, 44*, 7645-7658.

(53) Chen, A.; Komura, M.; Kamata, K.; Iyoda, T. Highly Ordered Arrays of Mesoporous Silica Nanorods with Tunable Aspect Ratios from Block Copolymer Thin Films. *Adv. Mater.* **2008**, *20*, 763-767.

(54) Chinthamanipeta, P. S.; Lou, Q.; Shipp, D. A. Periodic Titania Nanostructures Using Block Copolymer Templates. *ACS Nano* **2011**, *5*, 450-456.

(55) Hong, A. J.; Liu, C. C.; Wang, Y.; Kim, J.; Xiu, F.; Ji, S.; Zou, J.; Nealey, P. F.; Wang, K. L. Metal Nanodot Memory by Self-Assembled Block Copolymer Lift-Off. *Nano Lett.* **2010**, *10*, 224-229.

(56) Chuang, W. T.; Sheu, H. S.; Jeng, U. S.; Wu, H. H.; Hong, P. D.; Lee, J. J. Tetragonally Perforated Layer Structure via Columnar Ordering of 4´-(3,4,5-Trioctyloxybenzoyloxy)benzoic acid in a Supramolecular Complex with Polystyrene-*block*-Poly(4-vinylpyridine). *Chem. Mater.* **2009**, *21*, 975-978.

(57) Chuang, W. T.; Huang, Y. S.; Su, C. J.; Jeng, U. S.; Sheu, H. S. Successive Order–order Transitions of the Hierarchical Morphology of a Dendron-Jacketed Block Copolymer *via* Subsequent Stretching Alignment and Self-assembly. *Soft Matter* **2012**, *8*, 11163-11168.

(58) Chuang, W. T.; Lo, T. Y.; Huang, Y. C.; Su, C. J.; Jeng, U. S.; Sheu, H. S.; Ho, R. M. Directing the Interfacial Morphology of Hierarchical Structures of Dendron-Jacketed Block Copolymers via Liquid Crystalline phases. *Macromolecules* **2014**, *47*, 6047-6054.

(59) Lee, J. W.; Orolall, M. C.; Warren, S. C.; Kamperman, M.; Disalvo, F. J.; Wiesner, U. Direct Access to Thermally Stable and Highly Crystalline Mesoporous Transition-Metal Oxides with Uniform Pores. *Nat. Mater.* **2008**, *7*, 222-228.

(60) Yan, M. D.; Harnish, B. A Simple Method for the Attachment of Polymer Films on Solid Substrates. *Adv. Mater.* **2003***, 15*, 244-248.

(61) Wang, Y.; Liu, J.; Christiansen, S.; Kim, D. H.; Gösele, U.; Steinhart, M. Nanopatterned Carbon Films with Engineered Morphology by Direct Carbonization of UV-Stabilized Block Copolymer Films. *Nano Lett.* **2008***, 8*, 3993-3997.

(62) Sun, Y. S.; Huang, W. H.; Liou, J. Y.; Lu, Y. H.; Shih, K. C.; Lin, C. F.; Cheng, S. L. Conversion from Self-Assembled Block Copolymer Nanodomains to Carbon Nanostructures with Well-defined Morphology. *RSC Adv.* **2015***, 5*, 105774-105784.

(63) Jang, Y. H.; Xin, X.;Byun, M.; Jang, Y. J.; Lin, Z.; Kim, D. H. An Unconventional Route to High-efficiency Dye-Sensitized Solar Cells via Embedding Graphitic Thin Films into TiO_2 Nanoparticle Photoanode. *Nano Lett.* **2012**, *12*, 479-485.

(64) Stein, G. E.; Kramer, E. J.; Li, X.; Wang, J. Layering Transitions in Thin Films of Spherical-Domain Block Copolymers. *Macromolecules* **2007,** *40,* 2453-2460.

(65) Stein,G. E.; Lee, W. B.; Fredrickson, G. H.; Kramer, E. J. Li, X.; Wang, J. Thickness Dependent Ordering in Laterally Confined Monolayers of Spherical-Domain Block Copolymers. *Macromolecules* **2007**, *40,* 5791-5800**.**

(66) Vogt, B. D.; Chavez, V. L.; Dai, M.; Arreola, M. R. C.; Song, L.; Feng, D.; Zhao, D.; Perera, G. M. Stein, G. E. Impact of Film Thickness on the Morphology of Mesoporous Carbon Films using Organic−Organic Self-Assembly. *Langmuir* **2011***, 27*, 5607-5615.

(67) Sakurai, S.; Hashimoto, T.; Fetters, L. J. Thermoreversible Cylinder−Sphere Transition of Polystyrene-*block*-Polyisoprene Diblock Copolymers in Dioctyl Phthalate Solutions. *Macromolecules* **1996***, 29*, 740-747.

(68) Villanueva-Cab, J.; Jang, S. R.; Halverson, A. F.; Zhu, K.; Frank, A. J. Trap-Free Transport in Ordered and Disordered TiO_2 Nanostructures. *Nano Lett.* **2014***, 14*, 2305-2309.

(69) Yan, X.; Liu, G.; Liu, F.; Tang, B. Z.; Peng, H.; Pakhomov, A. B.; Wong, C. Y. Superparamagnetic Triblock Copolymer/Fe_2O_3 Hybrid Nanofibers. *Angew. Chem. Int. Ed.* **2001**, *40*, 3593-3596.

(70) Yelamanchill, R. S.; Walther, A.; Müller, A. H. E.; Breu, J. Core-Crosslinked Block Copolymer Nanorods as Templates for Grafting $[SiMo_{12}O_{40}]^{4-}$ Keggin Ions. *Chem. Commun.* **2008**, *48*, 489-491.

(71) Nandan, B.; Horechyy, A. Hairy Core−Shell Polymer Nano-objects from Self-Assembled Block Copolymer Structures *ACS Appl. Mater. Interfaces* **2015**, *7*, 12539−12558

(72) Jeng, U. S.; Su, C. H.; Liao, K. F.; Chuang, W. T.; Lai, Y. H.; Chang, J. W.; Chen, Y. I.; Huang, Y. S.; Lee, M. T.; Yu, K. L.; Lin, J. M.; Liu, D. G.; Chang, C. F.; Liu, C. Y.; Chang, C. H.; Liang, K. S.A Small/Wide-Angle X-ray Scattering Instrument for Structural Characterization of Air-Liquid Interfaces, Thin Films and Bulk Specimens. *J. Appl. Cryst.* **2010**, *43*, 110-121.

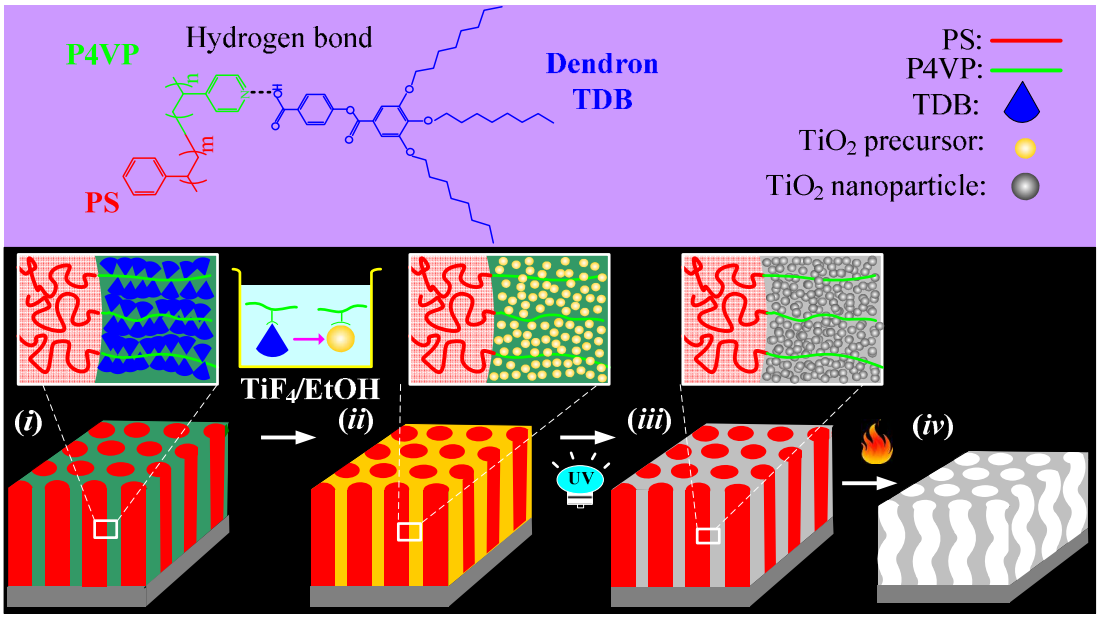

Figure 1. Schematic depicting the synthesis of vertically oriented mesoporous TiO_2 films using DJBCP templates following four steps: *i*) preparation of cylinder-forming DJBCP film; *ii*) migration of TiO_2 precursors to P4VP domains for guest exchange with dendrons upon immersion in a TiF_4/EtOH solution; *iii*) PS-*b*-P4VP/TiO_2 hybrids formed upon UV irradiation; and *iv*) formation of a mesoporous matrix of anatase TiO_2 after removal of the PS-*b*-P4VP host by calcination.

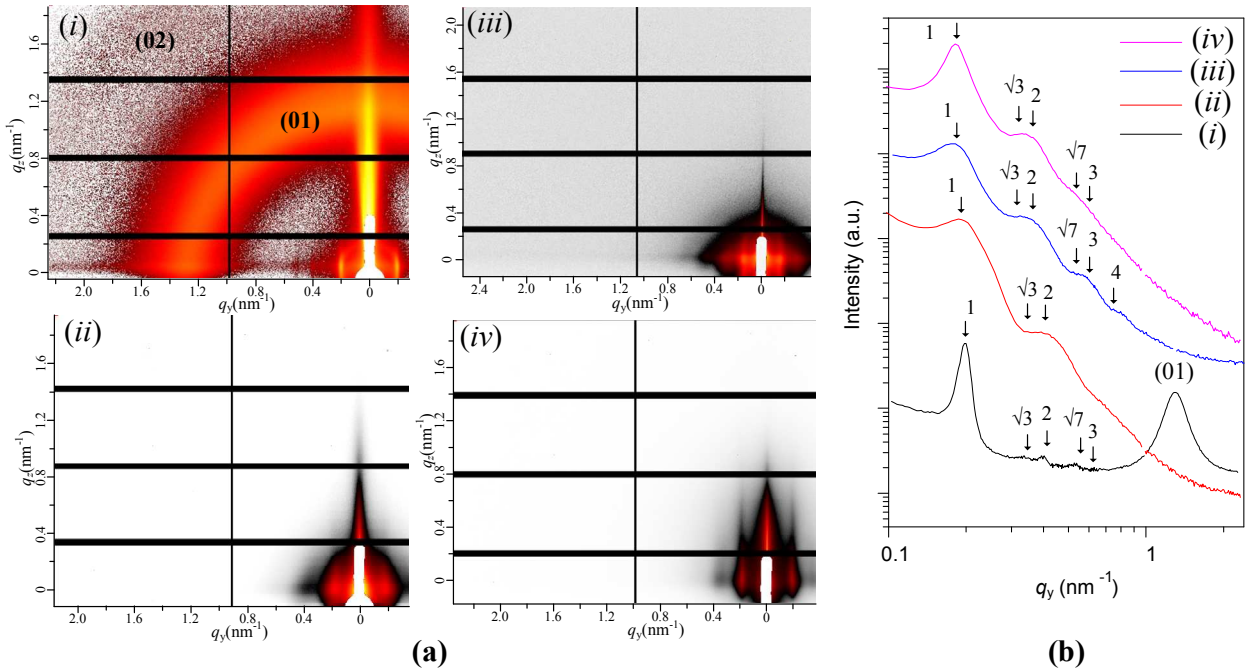

Figure 2. (a) 2D GISAXS patterns showing the structural evolution of vertically oriented mesoporous TiO_2 during the four-step synthesis (labeled as *i* to *iv*) illustrated in Figure 1. (b) The in-plane profiles corresponding to the peak position ratios of the ordered structures are indicated.

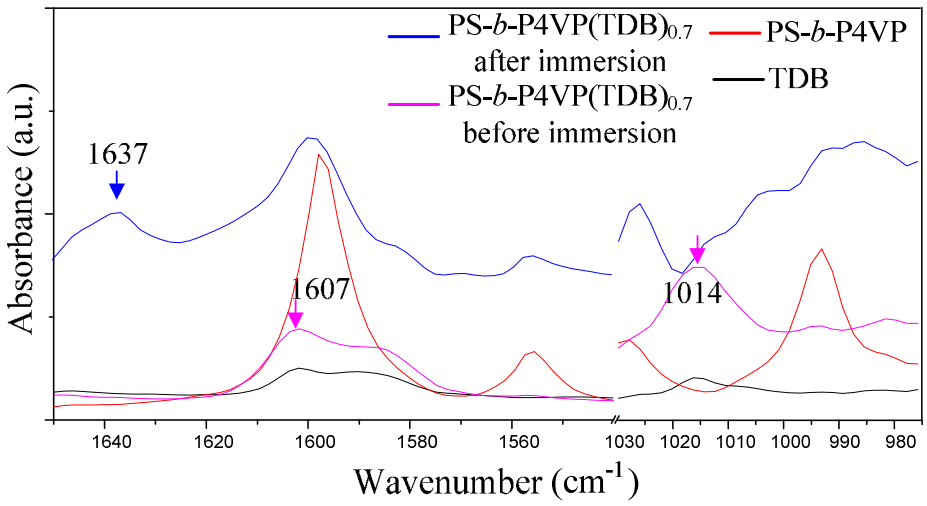

Figure 3. FTIR spectra for TDB, neat PS-*b*-P4VP, and PS-*b*-P4VP(TDB)$_{0.7}$ films before and after immersion in the precursor solution.

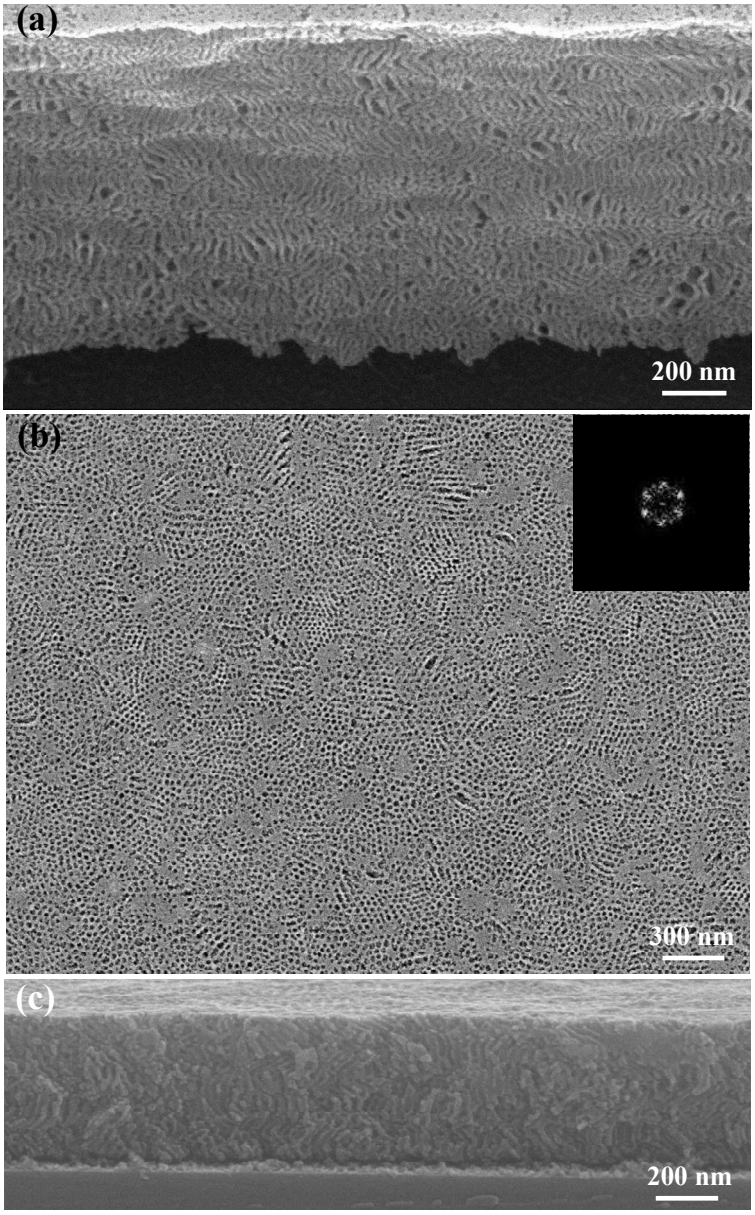

Figure 4. SEM images of (a) cross-sectional and (b) surface morphology of vertically oriented mesoporous TiO_2 film with 1 μm thickness; (c) cross-sectional SEM image of the mesoporous TiO_2 film 400 nm in thickness. Insert in (b) is 2D FFT image.

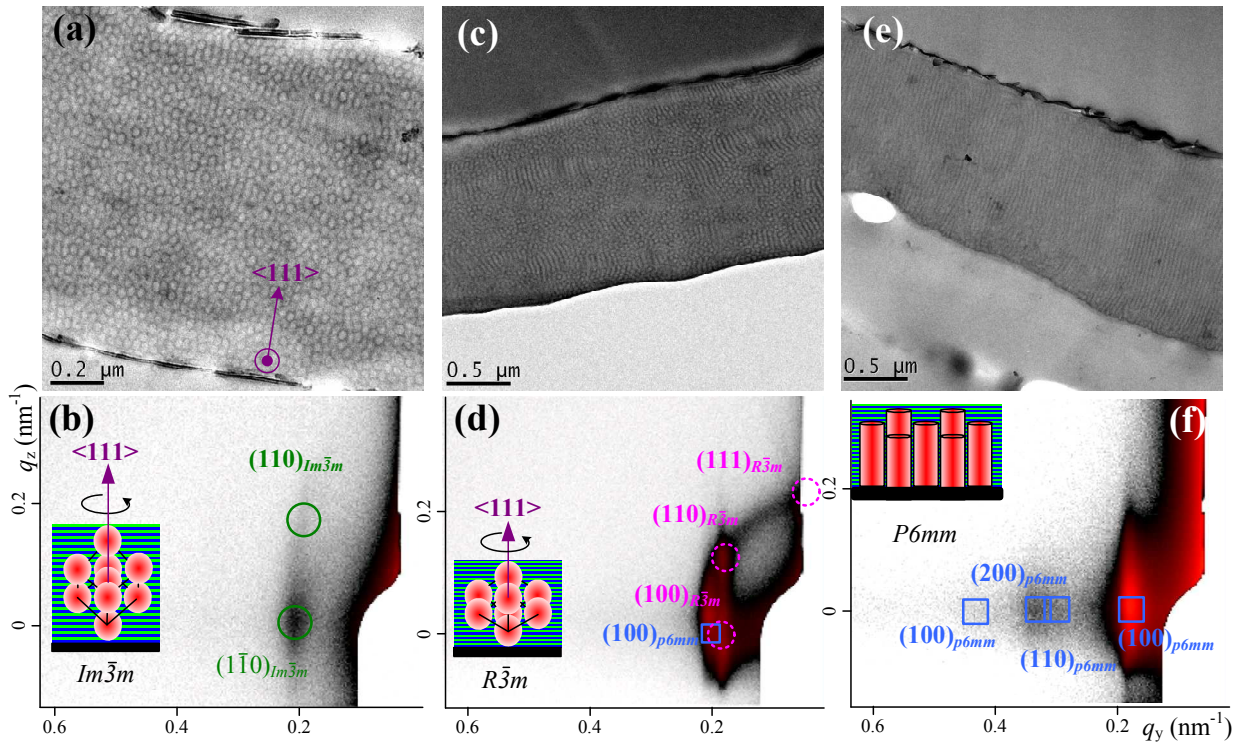

Figure 5. TEM images of the cross-sectional morphology (top) and 2D GISAXS patterns (bottom) of a PS-*b*-P4VP(TDB)$_{0.7}$ film from doctor-blade casting without annealing (a, b) and with (c, d) 2 h and (e, f) 15 h annealing. The dark zones in TEM images are I_2-stained P4VP microdomains.

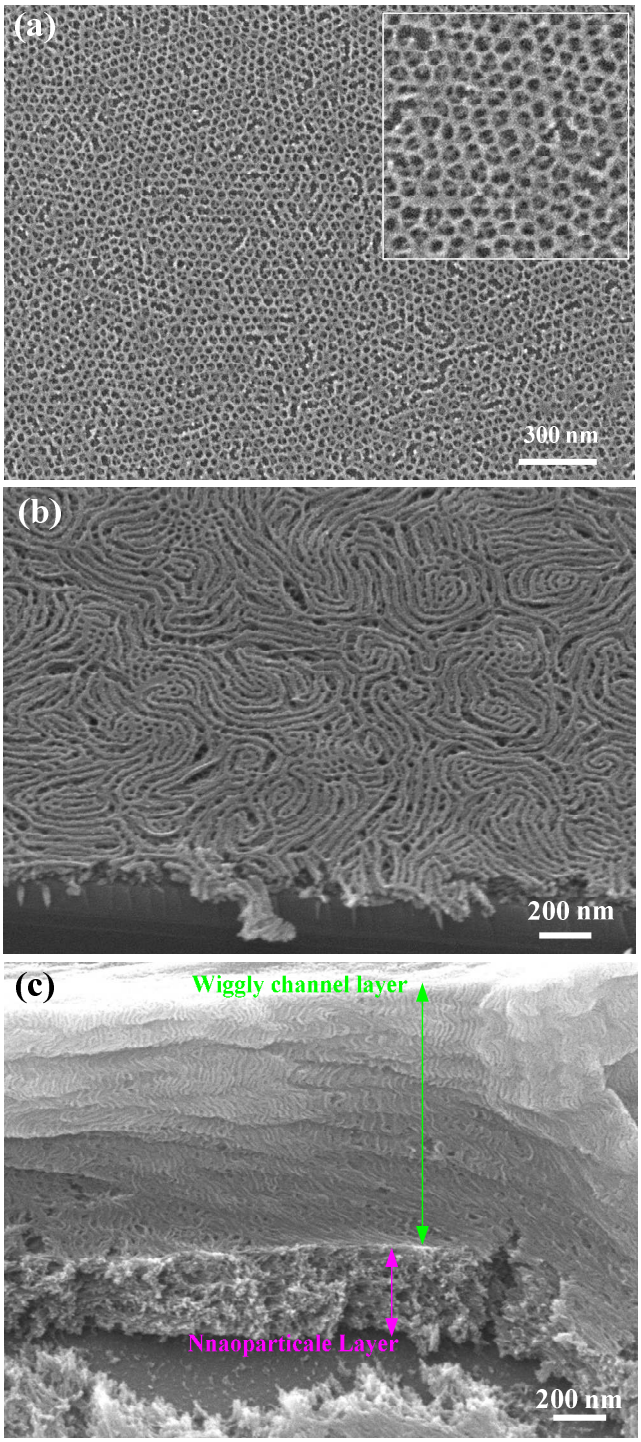

Figure 6. SEM images of (a) inverse opal-like TiO2 nanostructure (inset: high-magnification image, (b) fingerprint-like TiO_2 nanostructure with parallel channels, (c) cross-sectional morphology of the two-layer TiO_2 structure (top layer is vertically oriented mesoporous TiO_2 with wiggly channels and the bottom layer consists of TiO_2 P-25 nanoparticles).

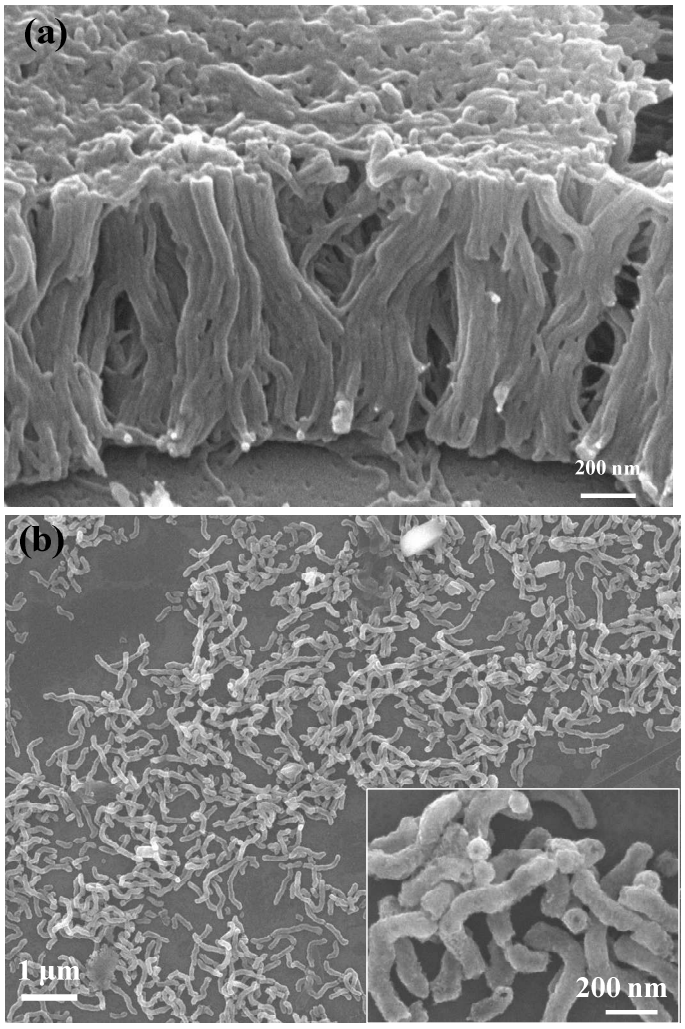

Figure 7. (a) SEM images of the morphology of pillars of PS-core@P4VP-shell after removal of TDB molecules upon immersion in cold ethanol without stir for 1 h; (b) TiO_2 nanotubes synthesized from the dispersed pillars and then calcination.
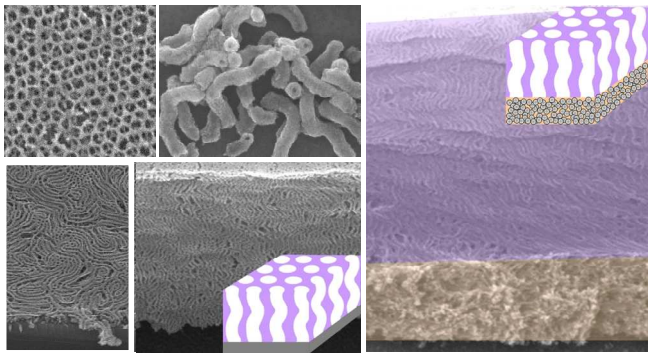
TOC graphic